Comparative Evaluation of AVIRIS-NG and Hyperion Hyperspectral Image for Talc Mineral Identification

Himanshu Govil, Mahesh Kumar Tripathi, Prabhat Diwan and Monika

Abstract The advancement and progressive development in hyperspectral remote sensing technology enhance the capability to measure the minor variations in spectral feature on the small and big scale of measurement. The remote sensing images provide information of earth's features according to the capability of regional coverage and larger synoptic view, but hyperspectral image provides detailed, subtle variation in the spectral resolution. In this study, Hyperion and AVIRIS-NG data were used for identification of talc mineral in and around the Jahazpur city, Chabhadiya village, India. The Hyperion hyperspectral data show absorption features of talc minerals but AVIRIS-NG minerals show the multiple absorption features with iron-bearing talc at the same location. In comparison, observed result shows that AVIRIS-NG has much accurate capability for identification of different minerals in the visible region along with the short-wave infrared portion of the electromagnetic spectrum.

Keywords AVIRIS-NG · Hyperion · Talc · Jahajpur · Spectroscopy

1 Introduction

On November 21, 2000, NASA launched push broom and sun-synchronous Hyperion hyperspectral sensor under the Earth observation (EO-1) mission. Hyperion hyperspectral remote sensing sensor became first hyperspectral spaceborne sensor [13]. Since its launch, Hyperion is only continuous source for hyperspectral remote sensing data in full coverage from 400 to 2500 nm of electromagnetic spectrum with 242 bands [15]. According to Mitchell et al. [13], the Hyperion has a problematic issue of cross track calibration and low signal-to-noise ratio.

In the success series of airborne and spaceborne hyperspectral remote sensing sensors such as AVIRIS and Hyperion, JPL NASA started a new mission of AVIRIS -NG [6] in the year 2014 in U.S.A. On achievement of positive result of AVIRIS-NG

H. Govil · M. K. Tripathi (✉) · P. Diwan · Monika
Department of Applied Geology, National Institute of Technology Raipur (C.G.), Raipur 492010, India
e-mail: tripathi.mahesh1@gmail.com

N. Sharma et al. (eds.), *Data Management, Analytics and Innovation*,
Advances in Intelligent Systems and Computing 1016,
https://doi.org/10.1007/978-981-13-9364-8_7

hyperspectral sensor in the USA, NASA-ISRO started a joint mission with some flight mission in India in the year 2016. On February 04, 2016, Jahajpur area of Bhilwara, Rajasthan, India was acquired by the airborne AVIRIS-NG hyperspectral sensor. ISRO-NASA has made a series of flights in that area for mineral identification [9, 16]. The image is captured by AVIRIS-NG sensor in 425 contiguous channels in spectral range of 0.38–2.51 μm including spectral resolution 5 nm and capability of high signal-to-noise ratio [2, 20].

According to various researchers [3, 8], the iron oxides/hydroxides and hydroxyl minerals which contain $Fe^{3+,}$ Mg-OH, Al-OH, SO_4, and CO_3 can be identified and mapped with the hyperspectral remote sensing data. On the basis of spectral characteristics, the EMR region is divided into two intervals such as VNIR and SWIR. VNIR interval ranges from 0.4 to 1.1 μm and SWIR interval ranges from 2.0 to 2.5 μm. Fe^{2+} and Fe^{3+} show electronic charge transfer absorption and crystal field absorptions in VNIR region and Al-OH, Mg-OH, CO_3, and SO_4 show vibrational OH and HOH overtones and stretches in SWIR region [3]. Kiran [10] described that the iron oxides/hydroxides such as goethite, limonite, and hematite show characteristic absorptions between 0.845 and 0.95 μm but hematite mineral is differentiated to other iron oxides on the basis of different absorptions features such as at 0.465, 0.650, and 0.850–0.950 μm. According to Meer ([12], the carbonate shows strong absorption at 2.3 and 2.35 μm (talc, calcite) and weaker absorption 2.12–2.16, 1.85–1.97, and 1.97–2.0 μm [12]. Meer [12, 21] suggested that talc shows the absorption at 2.3 μm due to Mg-OH. Meer et al. [21] have given description that in the SWIR region "vibration gives rise to narrow and more pronounced features roughly at 1.400 μm combined with 1.900 μm due to molecular water, 1.400 μm due to OH, 2.200 μm due to Al-OH, 2.300 μm due to Mg-OH, and 2.320–2.350 μm due to $CaCO_3$." Between the range of absorption, features of dolomite to calcite, epidote, talc, and pyrophyllite show absorption at 2.32, 2.33, 2.30, and 2.32 μm, respectively.

2 Geology of the Study Area

The geology of the Jahajpur area is classified in three zones named as Mangalwar complex situated in west from Archean basement of Jahajpur group, Hindoli group intruded the Archean basement rocks of Jahajpur groups in east, and two parallel dolomitic limestones and quartzite ride striking in NE–SW direction of Archean basement rocks along the river Banas. The main rocks of the Jahajpur group are quartzite, phyllite, banded iron formation (BIF), and quaternary sediments [7, 17–19, 23, 22] (Fig. 1).

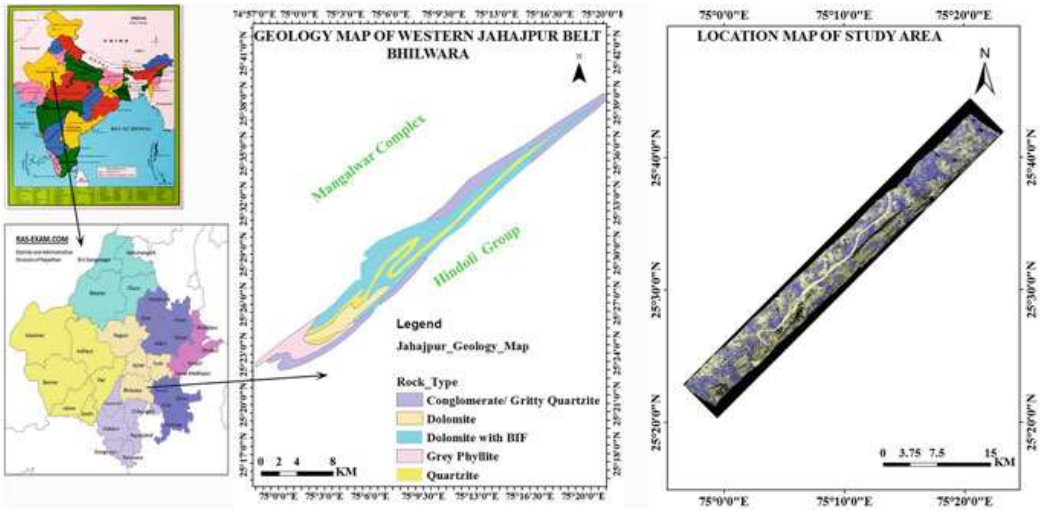

Fig. 1 Location and geology map of the study area [4, 9]

3 Materials and Methodology

The used scene of Hyperion hyperspectral remote sensing image have contiguous 242 narrow bands in the range of 0.4–2.5 μm with capability of spatial and spectral resolutions such as 30 m and 10 nm, respectively, with narrow swath coverage of 7.5 × 100 km including high radiometric accuracy of 12 bit quantization [1, 5, 11, 1214].

The AVIRIS-NG hyperspectral remote sensing data have 425 narrow contiguous bands in spectral region of VNIR and SWIR ranging from 0.38 to 2.51 μm of electromagnetic spectrum. The spatial and spectral resolutions are 8.1 m and 5 nm, respectively [2, 6, 9, 16]. The adopted methodology for mineral identification is divided into three parts such as pre-image processing, extraction of mineral spectra, and validation. The stage of prefield-image processing contains de-striping, bad band removal, and atmospheric correction. The second stage related to extraction of mineral spectra through image. Third stage involves in matching of image-extracted spectra and measured spectra of minerals through USGS mineral library spectra and with field samples spectra. There are 155 bands and 390 bands were found suitable for mineral identification and extraction of spectra by Hyperion and AVIRIS-NG hyperspectral image, respectively (Fig. 2).

4 Result and Discussion

The comparative analysis of extracted spectra of talc mineral by Hyperion hyperspectral remote sensing image of Chabhadiya area of Jahajpur, Bhilwara, Rajasthan shows diagnostic absorption features at 2.31 μm due to Mg-OH [3, 5, 12, 21]. Absorptions

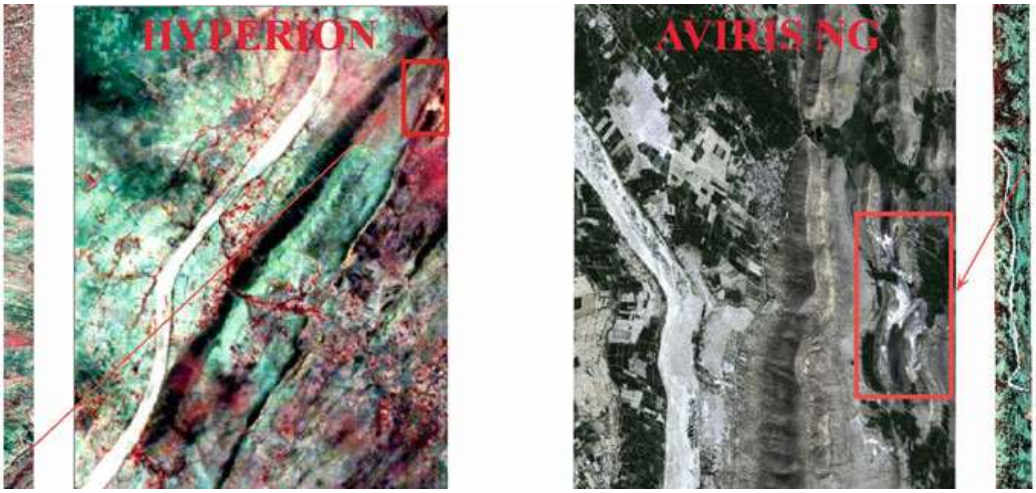

Fig. 2 Hyperion and AVIRIS-NG imagery

present at 1.4 and 1.9 μm due to OH and HOH overtones. There is some minor absorption also presents between 2.0 and 2.2 μm. In spectral range of 0.4–2.5 μm, some major absorption such as at 0.45 μm due to Fe^{3+} and at 0.9 μm, 1.1 μm due to O_2 and H_2O also identified in VNIR region of EMR. The Hyperion image spectra showing deep absorption at 0.85–0.95 μm which is indication of the presence of hematite [24] and showing normal absorption at near 0.456 μm [10]. The spectral analysis of AVIRIS-NG extracted talc mineral spectra shows diagnostic absorption at 2.31 μm with doublet 2.29 μm due to Mg-OH, and 1.4 and 1.9 due to overtones of OH and HOH. At near 1.4–1.5 μm and 2.0 μm shows maximum variation in absorption due to O_2 and CO_2 which is not present in the Hyperion image. Absorption at 0.47 and 0.6 μm indicating the presence of Fe^{3+}, (Hematite) and lesser deep absorption at 0.9 μm which is unavailable in Hyperion image. Various minor absorptions are also present minutely compared to minor absorption features of Hyperion image. The shape and reflectance value are also differentiating the characteristics and properties of both spectra. The subtle changes and subtle variation in shape, reflectance, and absorption can be observed very minutely in AVIRIS-NG than the Hyperion image. The spectroscopic spectra of talc field samples also validating the potential and capability of identification of talc and hematite with absorption at 2.31 μm with doublet at 2.28 μm with overtones of OH and HOH at 1.4 and 1.9 μm and Fe^{3+} presence identified at absorptions at near 0.56 and 0.9 μm, respectively. The shape, absorption, reflectance, and depth of image spectra of Hyperion and AVIRIS-NG in correlation of spectroscopic result of field sample spectra including comparison with USGS talc minerals spectra shows the most accurate and acute capability and performance of AVIRIS-NG hyperspectral images. The USGS talc mineral library spectra show complete matching of identified and measured spectra of talc through Hyperion, AVIRIS-NG, and spectroscopic field sample spectra (Fig. 3).

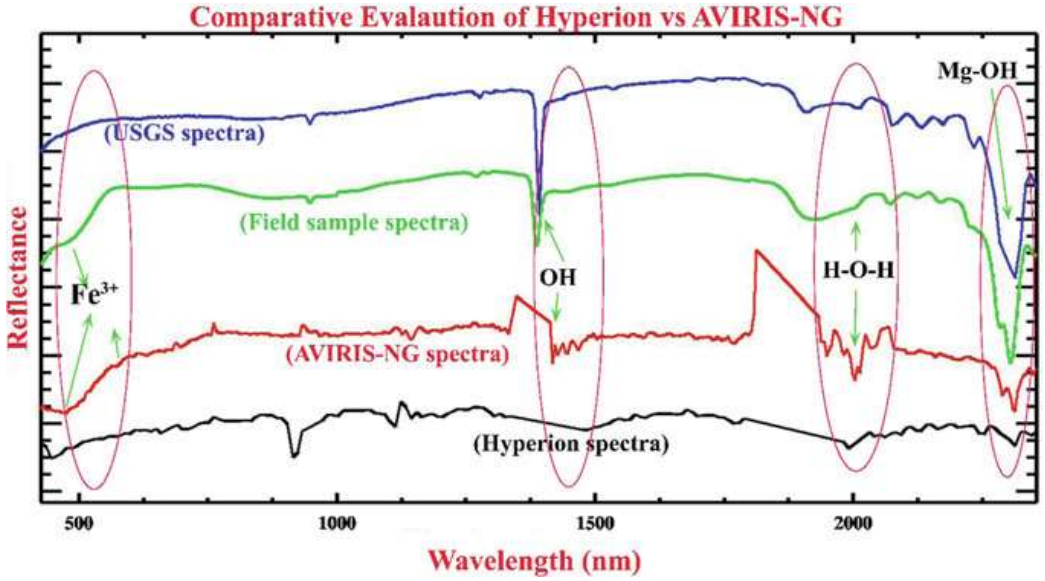

Fig. 3 Comparative evaluation of spectral profile of Chabhadiya talc mineral

5 Conclusion

The observed spectra of USGS talc mineral identified spectra of talc minerals through Hyperion and AVIRIS-NG and measured spectra of talc field sample by spectroscopy show the variation in absorption and reflectance. The AVIRIS-NG and field sample spectra show the presence of hematite in talc mineral spectra, but Hyperion talc mineral spectra have only capability to identify the presence of talc minerals. Some minor absorptions and range of absorptions also vary with subtle shift (changes) in absorptions. USGS talc mineral spectra validating the capability of identification of talc minerals through Hyperion and AVIRIS-NG but shows maximum similarity with AVIRIS-NG compared to Hyperion image. These comparative analytical results show that coarse spatial, spectral resolution, and low signal-to-noise ratio of Hyperion is unable to identify the minor absorption features of other minerals such as hematite in talc minerals, but AVIRIS- NG fine spatial and spectral resolutions and higher signal-to-noise ratio show capability and potential of the presence of minor minerals concentration with major minerals and their abundance. The observed result measured field sample spectra also verifying the potential and capability of AVIRIS-NG compared to Hyperion hyperspectral remote sensing data.

Acknowledgements This work is supported by Space Application Centre, Indian Space Research organization India grant EPSA/4.2/2O17.

References

1. Agar, B., & Coulter, D. (2007). Remote sensing for mineral exploration—A decade perspective 1997–2007 plenary session : The leading edge. In B. Milkereit (Ed.), *Proceedings of Exploration 07: Fifth Decennial International Conference on Mineral Exploration* (pp. 109–136).
2. Bhattacharya, B. K. (2016). *AVIRIS programme and science plan*. No. February, 18–22.
3. Clark, R. N. (1999). *Spectroscopy of rocks and minerals, and principles of spectroscopy. Remote sensing for the earth sciences: Manual of remote sensing* (Vol. 3). https://doi.org/10.1111/j.1945-5100.2004.tb00079.x.
4. Dey, B., Das, K., Dasgupta, N., Bose, S., & Ghatak, H. (2016). Zircon U-Pb SHRIMP dating of the Jahazpur granite and its implications on the stratigraphic status of the Hindoli-Jahazpur group. In *Seminar Abstract Volume: Developments in Geosciences in the Past Deca*.
5. Ducart, D. F., Silva, A. M., Toledo, C. L. B., de Assis, L. M., Ducart, D. F., Silva, A. M., Toledo, C. L. B., et al. (2016). Mapping iron oxides with Landsat-8/OLI and EO-1/Hyperion imagery from the Serra Norte iron deposits in the Carajás mineral province, Brazil. *Brazilian Journal of Geology, 46*(3), 331–49. (Sociedade Brasileira de Geologia). https://doi.org/10.1590/2317-4889201620160023.
6. Hamlin, L., Green, R. O., Mouroulis, P., Eastwood, M., Wilson, D., Dudik, M., & Paine, C. (2011). Imaging spectrometer science measurements for terrestrial ecology: AVIRIS and new developments. In *IEEE Aerospace Conference Proceedings*, No. August. https://doi.org/10.1109/AERO.2011.5747395.
7. Heron, A. M. (1935). Synopsis of the Pre-Vindhyan Geology of Rajputana. *Trans. Nat. Instt. Sci. India. I*, 17–33.
8. Jing, C., Bokun, Y., Runsheng, W., Feng, T., Yingjun, Z., & Dechang, L. (2014). Regional-scale mineral mapping using ASTER VNIR/SWIR data and validation of reflectance and mineral map products using airborne hyperspectral CASI/SASI Data. *International Journal of Applied Earth Observations and Geoinformation, 33*, 127–141 (Elsevier B.V.). https://doi.org/10.1016/j.jag.2014.04.014.
9. JPL NASA. (2015). *ISRO - NASA AVIRIS – NG Airborne Flights over India sciene plan document for hyperspectral remote sensing*.
10. Kiran Raj, S., Ahmed, S. A., Srivatsav, S. K., & Gupta, P. K. (2015). Iron Oxides mapping from E0-1 hyperion data. *Journal of the Geological Society of India, 86*(6), 717–725. https://doi.org/10.1007/s12594-015-0364-7.
11. Kruse, F. A., Boardman, J. W., & Huntington, J. F. (2003). Comparison of airborne hyperspectral data and EO-1 hyperion for mineral mapping. *IEEE Transactions on Geoscience and Remote Sensing, 41*(6 PART I), 1388–1400. https://doi.org/10.1109/TGRS.2003.812908.
12. Meer, F. V. (2004). Analysis of spectral absorption features in hyperspectral imagery. *International Journal of Applied Earth Observation and Geoinformation, 5*(1), 55–68.
13. Mitchell, J. J., Shrestha, R., Spaete, L. P., & Glenn, N .F. (2015). Combining airborne hyperspectral and LiDAR data across local sites for upscaling shrubland structural information: Lessons for HyspIRI. *Remote Sensing of Environment, 167*, 98–110 (Elsevier Inc.). https://doi.org/10.1016/j.rse.2015.04.015.
14. Pargal, S. (2011). *Hyperspectral subspace identification and endmember extraction by integration of spatial-spectral information*. University of Twente.
15. Pour, A. B., & Hashim, M. (2014). Exploration of gold mineralization in a tropical region using Earth Observing-1 (EO1) and JERS-1 SAR Data : A case study from Bau Gold Field, Sarawak, Malaysia, *1*, 2393–2406. https://doi.org/10.1007/s12517-013-0969-3.
16. SAC, ISRO. (2016). Space application Center.Pdf. SAC COURIER, *41*(3). http://www.sac.gov.in/SACSITE/SACCourier/July2016.pdf.
17. Saxena, A. S. H. A., & Pandit, M. K. (2012). Geochemistry of Hindoli group metasediments, SE Aravalli Craton, NW India : Implications for palaeoweathering and provenance. *Journal Geological Society of India, 79*, 267–278. http://mecl.gov.in/Reports/EXE_SUMM_BANERA.pdf.

18. Shekhawat, L.S., & Sharma, V. (2001). *Basemetal exploration in Pachanpura-Chhabbriya Block, Umedpura-Manoharpura Block, Gelaji (East) and Amargarh Blocks, Jahajpur Belt, Bhilwara District, Rajasthan* (Final Report For The Field Seasons 1999–2000 & 2000–2001).
19. Sinha Roy, S., &Malhotra, G. (1988). Structural relations of proterozoic cover and its basement: An example from the Jahazpur Belt, Rajasthan. *Jour. Geol. Sec. India* (in Press).
20. Thorpe, A. K., Frankenberg, C., Aubrey, A. D., Roberts, D. A., Nottrott, A. A., Rahn, T. A., et al. (2016). Mapping methane concentrations from a controlled release experiment using the next Generation Airborne Visible/Infrared Imaging Spectrometer (AVIRIS-NG). *Remote Sensing of Environment, 179,* 104–115. https://doi.org/10.1016/j.rse.2016.03.032. (Elsevier Inc.).
21. van der Meer, F. D., Harald, M. A., van der Werff, van Ruitenbeek, F. J. A., Hecker, C. A., Bakker, W. H., et al. (2012). Multi- and hyperspectral geologic remote sensing: A review. *International Journal of Applied Earth Observation and Geoinformation, 14*(1), 112–128. https://doi.org/10.1016/J.JAG.2011.08.002.
22. Yadav, S. K., & Rao, R. S. (2009). Assessment of iron ore potentiality of Jahazpur Belt, Central Rajasthan—A case study. *Geological Survey of India, 128*(3239), 885–886. https://doi.org/10.1038/128885a0.
23. Yadav, O. P., Babu, T.B., Shrivastava, P.K., Pande, A. K., & Gupta, K. R. (2001). Short communications and its significance in West Jahajpur Basin, Bhilwara District, Rajsthan. *Journal Geological Society of India, 58*, 0–3.
24. Zhang, T., Yi, G., Li, H., Wang, Z., Tang, J., Zhong, K., Li, Y., et al. (2016). Integrating data of ASTER and Landsat-8 OLI (AO) for hydrothermal alteration mineral mapping in Duolong Porphyry Cu-Au deposit, Tibetan Plateau, China. *Remote Sensing, 8*(11). https://doi.org/10.3390/rs8110890.